Moxon-Rae setup for the measurement of stellar (n,γ) rates and the example of ^{87}Rb

S. Jaag and F. Käppeler
Forschungszentrum Karlsruhe, IK-III, Postfach 3640, D-76021 Karlsruhe, Federal Republic of Germany
(Received 12 September 1995)

A setup with Moxon-Rae detectors was optimized for measurements of (n,γ) cross sections in the keV region. The experimental technique makes use of the quasi-Maxwellian spectrum that can be obtained via the ^{7}Li$(p,n)^{7}$Be reaction and is particularly suited for the determination of Maxwellian-averaged cross sections for nucleosynthesis studies related to *s*-process scenarios. It allows measurements at extremely short flight paths with the time-of-flight method as an option for background reduction. The experimental determination of the efficiency with calibrated γ sources and with two-step cascades from selected resonances of the ^{34}S (p,γ) reaction revealed new properties of the response function. The reliability of the method was first demonstrated at the example of the well-known ratio of the (n,γ) cross sections of Ta and Au, and then used for a measurement of the stellar ^{87}Rb cross section. With this new value $\langle\sigma v\rangle/v_T = 15.5 \pm 1.5$ mb, a discrepancy in the previously existing data could be resolved. [S0556-2813(96)04805-4]

PACS number(s): 25.40.Lw, 27.50.+e, 29.40.Ym, 97.10.Cv

I. INTRODUCTION

The origin of the heavy elements with $A>60$ must be ascribed to neutron capture reactions in the *s* and *r* processes. The rapid neutron capture process (*r* process) is associated with an explosive scenario and occurs presumably in supernovas [1,2]. For this process, reliable quantitative models are not available yet because of the uncertainties in the nuclear physics data, which are required for the involved nuclei on the *r*-process path close to the neutron drip line, and also due to the problems in modeling the explosion itself. These difficulties are much less severe for the slow neutron capture process (*s* process) which occurs during helium burning in the late stages of stellar evolution [3] where (n,γ) reactions occur on a time scale of ≈ 1 yr, slow compared to typical beta decay times. Therefore, the reaction chain of the *s* process follows the stability valley, and the resulting abundances are determined by the respective stellar cross sections. The *s*-process neutrons are produced via (α,n) reactions on ^{13}C and/or ^{22}Ne and exhibit a thermal spectrum according to temperatures of $100–300\times10^{6}$ deg ($kT\approx 30$ keV) and neutron densities of a few 10^{8} cm^{-3}.

The main nuclear input data for *s*-process studies are Maxwellian-averaged neutron capture cross sections in the keV region [3], which are commonly obtained from differential data in the energy range $1<E_n<250$ keV. One of the techniques for measuring these data is the time-of-flight (TOF) method in conjunction with Moxon-Rae detectors for recording the prompt capture γ-ray cascade [4–6]. Based on these earlier setups, the following appealing features of Moxon-Rae detectors are optimized in the present approach.

(i) Because of their good time resolution, these detectors can be used for TOF measurements at very short neutron flight paths. In this way, a high neutron flux can be achieved at the sample position which allows the determination of very small cross sections or, alternatively, the use of very small samples. This latter aspect is particularly important in the study of radioactive isotopes relevant for *s*-process branchings [3] in order to keep the radiation hazard at a manageable level.

(ii) Moxon-Rae detectors exhibit almost negligible efficiency at low γ-ray energies ($E_\gamma<0.5$ MeV), another advantage for reducing the background from a radioactive sample.

Moxon-Rae detectors [7] consist of a converter, typically of carbon or bismuth, to ''convert'' the capture γ rays into electrons by Compton scattering, pair production, or the photo effect. These electrons are either absorbed in the converter or detected in a thin plastic scintillator, which is mounted between the converter and a photomultiplier (Fig. 1). The efficiency ϵ_γ of such a detector increases almost linearly with γ-ray energy. This property results in an efficiency for neutron capture events, $\epsilon_{\rm capt}$, which is nearly proportional to the neutron binding energy S_n and independent of the capture γ-ray cascade $I_\gamma(E)$ [4,7].

In measurements with Moxon-Rae detectors, the main systematic uncertainty is due to deviations from the ideal proportionality between ϵ_γ and E_γ. Therefore, the slope of the efficiency curve was measured for three detectors with different converters. In this procedure, calibrated γ-ray sources were used up to 2.6 MeV. At higher energies, monoenergetic γ rays were selected from two-step cascades following resonant proton captures in ^{34}S by a coincidence with a HPGe detector. With these data, a reliable efficiency correction could be derived for the analysis of the subsequent cross section measurements.

The construction of the new detectors and the efficiency measurements are presented in Sec. II. In Sec. III, the reli-

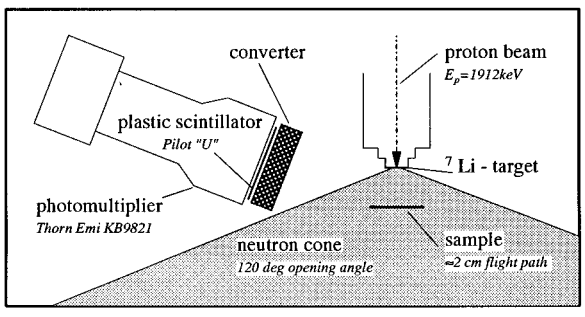

FIG. 1. Schematic sketch of the experimental setup.

ability of the method is verified by a measurement of the well-known cross section ratio of ^{181}Ta and ^{197}Au, where the results of Wisshak *et al.* [8] could be reproduced at a confidence level of about 5%. Eventually, the technique is applied to the determination of the small stellar (n,γ) cross section of the neutron magic nucleus ^{87}Rb (Sec. IV).

II. MOXON-RAE DETECTORS

For the intended use in TOF experiments at very short flight paths and for the investigation of radioactive samples, the detector components should meet the following requirements.

(i) *Converter*. Only converter materials with small neutron capture cross sections are to be used to minimize backgrounds in (n,γ) experiments. The converter thickness should be restricted to the maximum range of secondary electrons, that is, defined by the neutron binding energy of the investigated nuclei [7].

(ii) *Plastic scintillator*. Fast rise and decay times and an emission spectrum which fits the sensitivity profile of the photomultiplier are essential. The thickness of the scintillator must be a reasonable compromise between sufficient signal-to-noise ratio and low γ-ray sensitivity.

(iii) *Photomultiplier*. Apart from a fast rise time and a small dark current for achieving good time and energy resolution, the photomultiplier should exhibit a minimal response to γ rays in order to reduce distortions of the efficiency characteristics.

A. Construction and pulse height spectrum

The design of the Moxon-Rae detectors corresponds to the version described by Wisshak *et al.* [6], but is optimized with respect to time and energy resolution. The schematic sketch of Fig. 1 shows the relevant components. The combination of a 3 in. photomultiplier (Thorn EMI 9821KB) and a fast plastic scintillator (Pilot U, Nuclear Enterprise) yields a signal rise time of 2.7 ns as well as a good match of the scintillation light with the sensitivity maximum of the multiplier. The scintillator (diameter 50 mm, thickness 0.5 mm) is slightly smaller than the photocathode in order to avoid electrons from the outer region, which could deteriorate the time resolution. The scintillator is thin enough to minimize the response to γ rays, which are not absorbed in the converter, but sufficiently thick to ensure that the signal from the scintillator exceeds the γ-ray background of the multiplier itself. This background becomes particularly disturbing for multipliers with quartz windows, where it equals the effect from the scintillator even for γ rays in the MeV region.

The photomultiplier base and preamplifier are similar to the solution developed for the Karlsruhe 4π BaF_2 detector [9]. The modifications concern additional measures for suppression of noise and spurious signals because the Moxon-Rae response is about one order of magnitude smaller than the signals obtained from BaF_2 crystals.

In the present work, three different converters were used, all 56 mm in diameter. According to theoretical calculations [10–12], the best choice for the converter material was a mixture of graphite (11.4% by weight) and bismuth oxide, since it combines a low neutron capture cross section with an almost linear relation between efficiency and γ-ray energy. This mixture was pressed to a disk of 10 mm thickness. In addition, converters of pure graphite (20 mm thick) and metallic Bi (6 mm thick) were prepared for studying the systematic uncertainties due to deviations from the ideal response. A fourth converter was made of 5 mm thick metallic molybdenum, which is expected to exhibit an ideal linearity $\epsilon \sim E_\gamma$, [10] but which has a comparably large capture cross section for keV neutrons. Therefore, it was used to test the detector response for scattered neutrons.

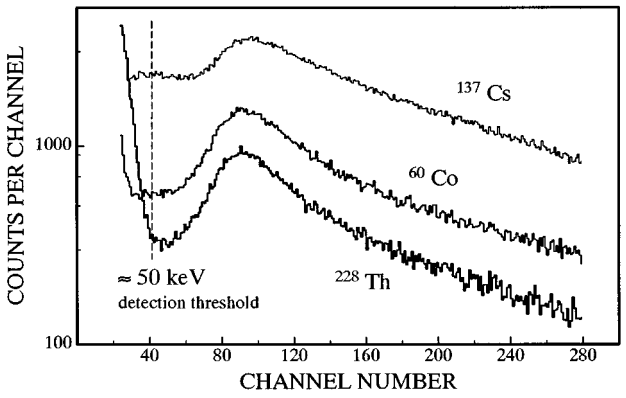

FIG. 2. Pulse height spectra of a Moxon-Rae detector for different γ-ray sources. The electronic threshold is adjusted in the minimum of the ^{60}Co spectrum around 50 keV as indicated.

Typical pulse height spectra of a Moxon-Rae detector are shown in Fig. 2 for different γ-ray sources. The quality of the present design is obvious from the deep minimum between multiplier noise and scintillator signals. This minimum is important for defining the electronic threshold and, hence, the detector efficiency.

B. Measurements of the detector efficiency

In all measurements of this work, the electronic threshold of the Moxon-Rae detectors was defined by the minimum in the pulse height spectrum obtained with the ^{60}Co source as indicated in Fig. 2. Furthermore, the same distance of about 8 cm between source and detector was chosen in the efficiency studies and in the subsequent TOF experiments.

Below 2.6 MeV γ-ray energy, the efficiency of the detectors was determined by means of calibrated sources. In addition to the monoenergetic lines from ^{85}Sr (0.514 MeV), ^{137}Cs (0.662 MeV), ^{54}Mn (0.834 MeV), and ^{65}Zn (1.115 MeV), the two-step cascades in the decay of ^{60}Co (1.173 and 1.332 MeV), ^{88}Y (0.898 and 1.836 MeV), and ^{228}Th (0.583 and 2.615 MeV) were used as well. In these cases, the coincident observation of the respective counterpart was required for identification of the detected γ ray. This was achieved with a 40 ccm HPGe detector, which was placed at an angle of 125° with respect to the detector axis. In this way, angular correlation effects could be avoided, since the Legendre polynomial $P_2(\cos\theta) = 0$ for $\theta = 125°$ (see Ref. [13] for a detailed discussion).

For energies above 2.6 MeV, two resonances of the $^{34}S(p,\gamma)^{35}Cl$ reaction were selected for the production of two-step cascades [14]: At $E_p = 1.212$ MeV one obtains γ rays of 4.380 and 3.158 MeV, and the second resonance at $E_p = 1.021$ MeV yields γ rays of 6.144 and 1.219 MeV.

The ^{34}S target of 80 μg/cm^2 thickness was prepared by vacuum deposition of ZnS on a tantalum disk [13]. The measurements were carried out at the Karlsruhe 3.75 MV Van de Graaff accelerator with proton beam currents of about 25 μA. The coincident observation was performed with the same arrangement as described above, but in this case a 175 ccm HPGe detector was used to achieve counting statistics of 3–4 % within typical measuring times of 12 h. For all two-step γ cascades the experimental count rates had to be corrected for contaminating coincident transitions as discussed in Ref. [13].

These measurements are summarized in Fig. 3. Data points from two-step cascades exhibit uncertainties of 3–6 % mainly due to counting statistics, while the uncertainties of the other data originate mainly from the activity uncertainties of the calibrated sources. In all cases, an additional contribution of 2% was considered for the uncertainties related to the counting geometry.

In the ϵ_γ/E_γ plot of Fig. 3, the ideal case of a linear response $\epsilon_\gamma \sim E_\gamma$ would appear as a horizontal line. For comparison, the theoretical values of Iyengar *et al.* [10] are given as well. Obviously, not only the absolute efficiency but also the slopes of the measured curves differ significantly from the theoretical predictions. The characteristic ''nose'' around $E_\gamma \sim 1$ MeV, which appears for all converter materials, was not noticed in the original work by Moxon and Rae [7], but was reported by Macklin *et al.* [4] and later confirmed by Corvi [15]. This effect was assumed to result from the contributions due to pair production and the photoelectric effect, which were not considered in the earlier work. However, when these processes were included in later calculations [10–12], this feature could not be reproduced either. Apart from the ''nose,'' the calculated curves are consistently flatter than was found experimentally.

These differences between measured and calculated γ-ray efficiencies translate into systematic differences for the detection efficiency of typical capture events, which can be as large as 10%. For further applications of Moxon-Rae detectors it was, hence, important to identify the origin of these discrepancies.

C. Interpretation of the Moxon-Rae efficiency

There are two problems which are common to all previous theoretical studies [10–12]: None of these models considered the *direct* interaction of γ rays passing through the converter, neither with the plastic scintillator nor with the photomultiplier. Moreover, all calculations were based on very old data [16] for describing low energy electron scattering in the converter.

With the simplifying assumption of normal incidence and neglecting γ-ray scattering in the converter and scintillator, the efficiency contribution from the scintillator can be approximated [17] by

$$\epsilon_{\text{scint}} = e^{-\mu D}(1 - e^{-\sigma \rho x}),$$

where μ denotes the γ-ray absorption coefficient of the converter, D the converter thickness, ρ the electron density of the scintillator (0.338×10^{24} cm^{-3}), and x the scintillator thickness of 0.5 mm. The effect of the detector threshold is considered via the threshold-dependent detection cross section σ [17]. For the present setup, where the threshold is defined in the minimum of the pulse height spectrum of a ^{60}Co source, corresponding to $\approx$50 keV electron energy, these cross sections are 0.1–0.2 b/electron.

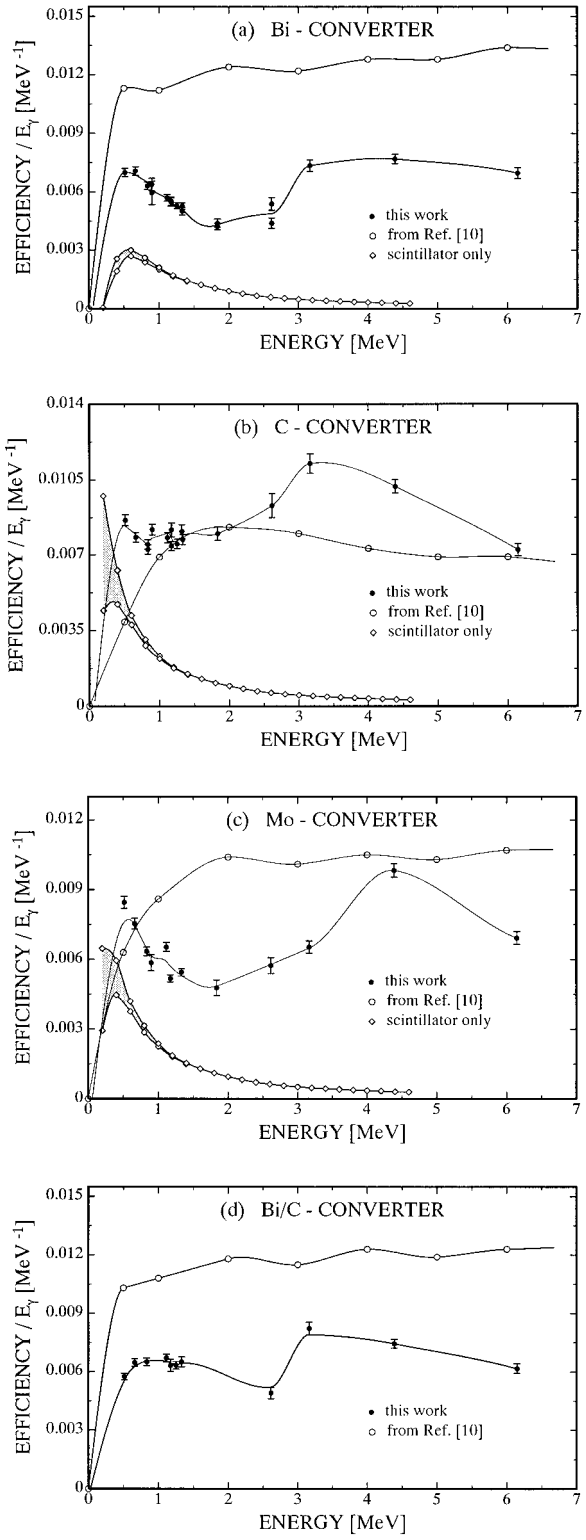

FIG. 3. (a)–(d) The measured ratio of detector efficiency and γ-ray energy for different converter materials. The ideal behavior corresponds to a horizontal line.

The result of this calculation is shown in Figs. 3(a)–3(c) by the open diamonds. The shaded band represents the esti-

TABLE I. Samples for the Ta measurement and related corrections.

		Samples		
		Au	Ta	Bi
Sample mass (g)		0.2968	0.8282	4.1548
Sample thickness (mm)		0.03	0.1	1.72
Sample diameter (mm)		25	25	25
Neutron binding energy S_n (MeV)		6.118	6.567	4.545
γ-ray self-absorption GA	Bi converter	0.994	0.985	0.929
	C converter	0.994	0.987	0.934
	Bi/C converter	0.995	0.988	0.938
Multiple scattering and self-shielding MS$\times$SS		1.0	1.005	1.025

mated uncertainty related to the detection threshold. Another uncertainty comes from the threshold-dependent detection cross section, particularly at lower energies, since no data are given below 300 keV [17]. Whereas these uncertainties are of minor importance for the Bi converter with its rather high absorption, it becomes relevant for the other two converter materials.

For the Bi converter the plastic scintillator response fits the characteristic *nose* of the measured detection efficiency quite well. The difference obtained for the C or Mo converters must be seen with respect to the uncertainties (as estimated by the shaded band) and/or may be due to the rather simple model assumptions.

Nevertheless, the qualitative agreement is evident and confirms that the Moxon-Rae efficiency in the energy region below 1.5 MeV is mainly determined by γ rays penetrating the converter and interacting directly with the scintillator. At higher energies, the efficiency is underestimated by the calculations since the direct interaction of γ rays with the photomultiplier itself were also not considered. This effect results in a steady increase of the efficiency with E_γ, independent of the converter material, and was verified in the above coincidence experiments with the converter removed from the detector.

In summary, it is important to note that *the efficiency of Moxon-Rae detectors is not only determined by interactions in the converter material, but also by non-negligible contributions from interactions in the scintillator and in the photomultiplier*. Since a reliable theoretical model is still missing, this means that the use of Moxon-Rae detectors for cross section measurements should include an experimental determination of their γ-ray efficiency.

III. MEASUREMENT OF THE ^{181}Ta CROSS SECTION

A detailed description of the experimental method, data evaluation, and discussion of the systematic uncertainties is already given in Refs. [5,6,18]. Therefore, a concise discussion of the main features may suffice here.

The measurements were carried out with neutrons from the Karlsruhe 3.75 MV pulsed Van de Graaff accelerator using the ^{7}Li$(p,n)^7$Be reaction for neutron production. The proton energy was adjusted slightly above the reaction threshold in order to obtain a kinematically collimated neutron beam in a forward cone of 120° opening angle. Integration over this cone yields a continuous neutron spectrum ranging from $\sim$1 keV to 106 keV, which represents a very good approximation of the stellar situation [19]. Three Moxon-Rae detectors with graphite, bismuth, and bismuth-graphite (or molybdenum) converters were mounted at an angle of 120° with respect to the proton beam, completely outside the neutron cone as indicated in the schematic setup of Fig. 1.

However, as indicated in Fig. 1, the sample did not cover the neutron cone completely. This has the consequence that the effective neutron spectrum, though peaked near 30 keV, becomes too narrow for a good approximation of a Maxwell-Boltzmann distribution. Therefore, the experimental TOF spectra have to be analyzed in a differential way.

A. Samples and related corrections

The measurement was performed with metallic samples of natural composition. In addition to the Ta sample, a gold sample was used for determining the neutron exposure, and a bismuth sample served for background determination. The samples were 25 mm in diameter, mounted on a vertical sample changer at a distance of 20 ± 0.1 mm from the neutron target. An empty position in the sample changer allowed us to derive the sample-independent background. During the experiment, the samples were changed cyclically into the measuring position in intervals of about 12 min by integrating the proton beam current to a preselected charge. These rather short intervals were chosen to avoid corrections for slow variations of the neutron flux. That all samples received the same neutron exposure was verified by means of an additional TOF spectrum recorded with a ^{6}Li glass detector at a flight path of about 1 m.

The relevant sample data of the tantalum measurement are listed in Table I together with the sample-related corrections for neutron multiple scattering and self-shielding and for γ-ray self-absorption. The corrections for neutron multiple scattering (MS) and self-shielding (SS) were calculated with the Monte Carlo code SESH [20]. Because of the relatively thin samples, these corrections and the related uncertainties are small. The values listed in Table I are averages over the quasistellar neutron spectrum of the experiment.

The correction for γ-ray self-absorption (GA) in the samples has been estimated using the total absorption coefficients $\mu(E_\gamma)$ of Storm and Israel [21]. The probability for a γ ray of energy E_γ to escape from the sample is

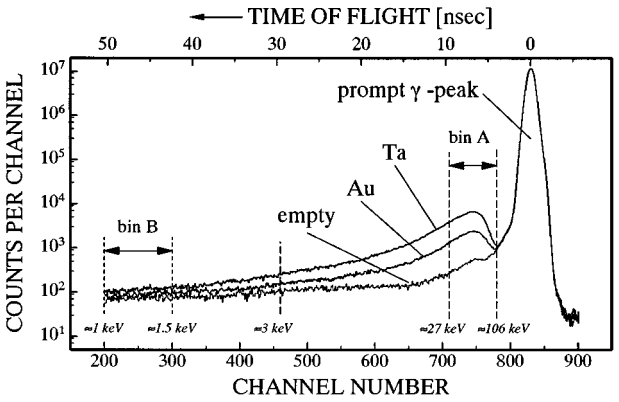

FIG. 4. Experimental TOF spectrum of the Ta/Au measurement.

$$p(E_\gamma)=\frac{1-\exp(-\mu d_{\rm eff})}{\mu d_{\rm eff}}.$$

The effective sample thickness, $d_{\rm eff}$ was twice the true sample thickness since the detectors were located at a backward angle of 120°. For capture events, the correction factor GA is obtained by folding with the energy-dependent detector efficiency ϵ_γ and with the capture γ-ray spectrum I_γ:

$$\mathrm{GA}=\frac{\int_0^{S_n} p(E_\gamma)\epsilon_\gamma I_\gamma dE}{\int_0^{S_n}\epsilon_\gamma I_\gamma dE}.$$

The capture γ-ray spectra were determined by statistical model calculations [22] as described in Refs. [8,23]. For Ta, the resulting correction is ~1% and exhibits only small differences for the different converters, which are, in fact, negligible for the thin Ta and Au samples.

B. Time-of-flight spectra

Figure 4 shows the time-of-flight (TOF) spectra of the Ta and Au samples together with the background spectrum obtained with the empty sample position. These spectra represent the sum over all detectors. In single runs, a time resolution of 800 ps could be achieved. The flight path was 20 ± 0.1 mm, the maximum neutron energy 106 keV, and the total measuring time 24 h, corresponding to 25 cycles. The TOF scale is defined by the prompt γ-ray peak from the impact of the proton pulse on the ^{7}Li target.

In order to correct for a long-term drift in the electronics, a small shift in the TOF scale was compensated by a linear transformation to a common position of the prompt γ-ray peak before the spectra of the individual cycles were combined to common TOF spectra. The differences in the integrated neutron exposure received by the various samples were determined from the neutron spectra of the ^{6}Li glass monitor by due consideration of the respective sample transmissions. Since these differences were always smaller than 0.5%, the related uncertainties could be neglected.

Analysis of the TOF spectra is complicated due to the close geometry between neutron target and sample for the following reasons.

(i) Neutrons from the edge of the target hitting the opposite edge of the sample travel a 26% longer flight path than the normal target-sample distance.

(ii) Differences in emission angle imply significant differences in neutron energy since the proton energy was close to the threshold of the ^{7}Li$(p,n)^7$Be reaction.

(iii) The average TOF is not very long compared to the experimental time resolution.

Altogether, these effects make it difficult to evaluate the measured TOF spectra in terms of neutron energy. Hence, TOF bins corresponding to the experimental time resolution instead of energy bins are preferred further on, but when used, energy values refer to a mean flight path of 22.5 mm.

Figure 5 shows the neutron energy spread for these bins. While the bins at low energies exhibit a reasonable resolution, those at high energies are considerably smeared out in neutron energy. Accordingly, the cross section information had to be deduced in a more indirect way as outlined in Sec. III.

C. Capture γ-ray spectra and efficiency correction

Since the Moxon-Rae efficiency differs from a linear increase with γ-ray energy, the detection probability of a capture event is not exactly proportional to the neutron binding energy S_n, and has to be corrected by considering the capture γ-ray spectrum $I_\gamma(E)$, the γ-ray efficiency $\epsilon_\gamma(E)$, and the self-absorption effects in the sample, $p(E)$. This correction is defined as

$$\zeta=\frac{\int_0^{S_n}\epsilon_\gamma p I_\gamma dE}{\int_0^{S_n} E p I_\gamma dE}.$$

The capture γ-ray spectra of ^{181}Ta and ^{197}Au were obtained by statistical model calculations at a neutron energy of 30 keV [8,23].

For comparison of the investigated isotope and the gold reference sample it is convenient to consider the ratio of the correction factors ζ,

$$\Delta_\epsilon(x)=\zeta(x)/\zeta(\mathrm{Au}).$$

Based on the experimental efficiency curves of this work, the $\Delta_\epsilon(x)$ values for the different converters may differ by up to 10%. The largest deviation is found for the Bi converter due to the pronounced drop in efficiency around 3 MeV. If the theoretical efficiency curves are used instead, there are striking differences compared to the present results (Table II).

The uncertainties due the calculated capture γ-ray spectra were estimated by comparing the $\Delta_\epsilon(x)$ values for the calculated gold spectra of Reffo *et al.* [23] and of Uhl and Kopecky [24] in the lower part of Table II. In this test, the largest deviations of about 4% were again obtained for the Bi converter. The observed differences for Δ_ϵ(Au) suggest a remaining systematic uncertainty of about 5%, which appears to be inherent to Moxon-Rae detectors, mainly due to the uncertainties in the calculated capture γ-ray spectra. Since the C converter exhibits the flattest response function (Fig. 3), this detector has the lowest sensitivity with respect to the capture γ-ray spectra and is, therefore, expected to give the best results, in striking contradiction to the calculations, which favored the Bi/C mixture.

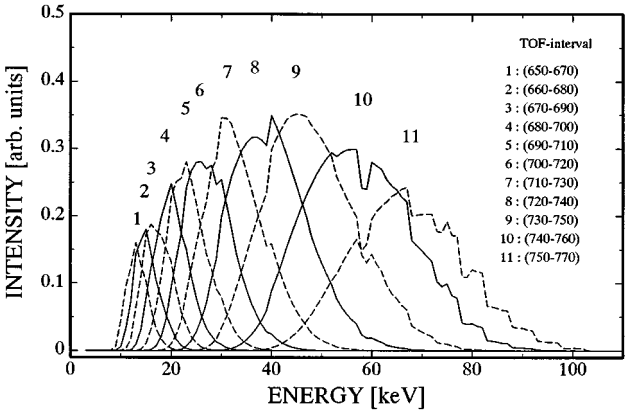

FIG. 5. Energy distributions for the various TOF bins discussed in the text [a Monte Carlo calculation based on measured neutron spectra from the ^{7}Li$(p,n)^{7}$Be reaction] [19].

D. Background subtraction

In addition to the tantalum sample and the gold reference sample, TOF spectra were also taken for an empty position to determine the sample-independent background, and for two scattering samples of metallic bismuth to study the effect of scattered neutrons. In this respect, Bi samples are particularly suited due to the large scattering to capture ratio of ^{209}Bi.

The correction for scattered neutrons is a crucial point for any TOF experiment. For the present setup this correction is quite different compared to high resolution measurements. The primary flight path being short compared to the distance between sample and γ-ray detectors allows one to exploit the difference in the TOF for the separation of capture γ rays and the scattered neutrons. Some of the background components from scattered neutrons is illustrated in the TOF spectrum of the Mo converter used in the measurement of the ^{87}Rb cross section (Fig. 9). Because of the geometry of the experimental setup, background from scattered neutrons can be excluded for the first TOF interval (bin *A* in Fig. 4). This background starts only at the TOF corresponding to a primary neutron energy of $\sim$27 keV, when the first sample-scattered neutrons reach the Cu backing of the Li target. At still later times the neutrons scattered in the target backing and in the sample are reaching the converters (indicated as ''target'' and ''sample'' in Fig. 9). At these later times, the background is smeared out in time compared to the primary yield and, hence, it is less sensitive to the structure of the scattering cross sections.

If one compares the TOF spectra of Fig. 9, the scattering background from the ^{209}Bi sample is very small down to channel 600 since there is no difference corresponding to the spectrum of the empty sample position. The scattering effect starts to be important at a later TOF, where the ^{209}Bi spectrum merges with that of ^{87}Rb. However, this TOF interval is no longer used for analysis. This suppression of the scattering background is confirmed by the later discussed cross section plot of Fig. 10, which shows that the results obtained with the three Moxon-Rae detectors start to deviate from each other only below channel 620: This behavior is to be expected since the detector response to scattered neutrons differs due to their different converters and their different location in the setup. In summary, the assumption that the scattering correction is independent of neutron energy (or TOF) appears well justified.

The scattering correction was obtained in the following ways.

(i) At primary neutron energies below $\sim$1.5 keV (time bin *B* in Fig. 4), true capture events in the sample can be neglected compared to the scattering background since the experimental neutron spectrum is restricted to the range between 1 keV and 106 keV due to the kinematics of the ^{7}Li$(n,p)^{7}$Be reaction, and since the yield at the lower end of the spectrum is almost negligible, the total count rate C_x in bin *B* was used to calculate the relative scattering intensity f of the sample x:

$$f_x=(C_x-C_{\text{empty}})/(C_{\text{Bi}}-C_{\text{empty}}).$$

Below 1.5 keV these f_x values were almost independent of the TOF interval from which they were determined.

(ii) Alternatively, the f_x values can be estimated directly via the average scattering cross sections between 70 and 90 keV. Given the geometry of the setup this energy interval is expected to contribute most to the scattering background of the evaluated TOF bins.

Both sets of f_x values were found in good agreement but, more important, it turned out that the final cross section results are almost insensitive to the ways of calculating f_x, the remaining differences being comparable to the statistical uncertainties.

However, capture events in the scattering sample cannot be neglected at higher energies. This means that the count rates in the TOF spectrum of the Bi scattering sample had to be corrected for true captures. This was done by normalizing the measured effect in the scattering free energy interval of

TABLE II. Efficiency corrections for the Ta measurement.

		Converters		
Reference		Bi	Bi/C	C
			Δ_ϵ(Ta), I_γ of Ref. [23]	
This work	expt. ϵ_γ	1.096	1.035	1.001
Iyengar *et al.* [10]	theor. ϵ_γ	1.019	1.016	0.974
			Δ_ϵ(Au), I_γ of Ref. [24]	
This work	expt. ϵ_γ	1.04	1.021	1.0006
Iyengar *et al.* [10]	theor. ϵ_γ	1.004	0.999	0.981

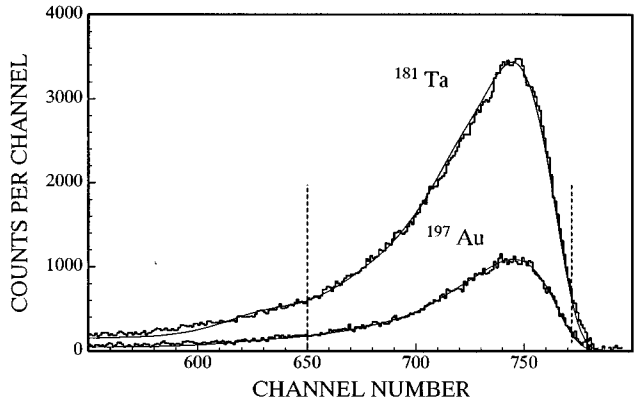

FIG. 6. The experimental TOF spectra of the Ta and Au samples taken with the Bi converter (histograms) compared to the Monte Carlo simulations (solid lines). The relevant TOF region used for cross section analysis is indicated by dashed lines (see text).

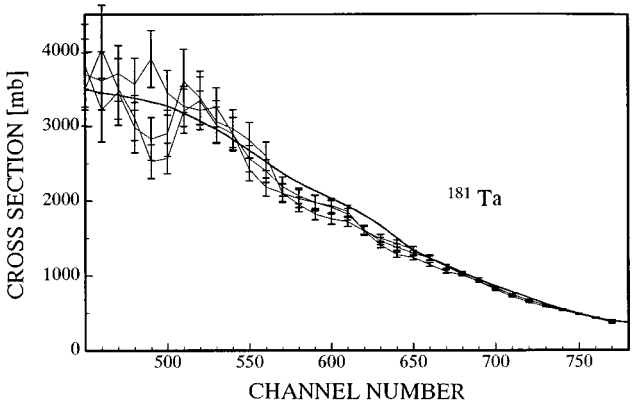

FIG. 7. The measured neutron capture cross sections for the whole TOF spectrum. The thick solid line indicates the curve expected from the precise measurement of Wisshak *et al.* [8]. Error bars correspond to statistical uncertainties only.

bin A to the capture cross section of Bi, making use of the differential data given by Macklin and Halperin [25] (for more details see Refs. [26,27]).

The capture rate in the scattering free energy interval can also be used to derive the ^{209}Bi cross section. This result was found to be in perfect agreement with a previously reported dedicated experiment [26,27].

E. Results

The ratios of the capture cross sections of tantalum and gold were determined for the different converters by the relation

$$\frac{\sigma_{\mathrm{Ta}}}{\sigma_{\mathrm{Au}}}=\frac{C_{\mathrm{Ta}}(N\times S_n\times \mathrm{MS}\times \mathrm{SS}\times \mathrm{GA})_{\mathrm{Au}}}{C_{\mathrm{Au}}(N\times S_n\times \mathrm{MS}\times \mathrm{SS}\times \mathrm{GA})_{\mathrm{Ta}}}\Delta_\epsilon,$$

where C are the background-corrected counts in the TOF spectrum, and N the number of sample nuclei. However, as discussed above, differential data cannot be extracted directly due to the poor energy resolution of the experiment. Instead, integral cross section ratios were determined for different overlapping TOF bins having a width of 20 channels (compare tabular inset in Fig. 5).

The easiest way of comparing the present results with the precise data of Wisshak *et al.* [8] is to use the differential capture cross sections of Au and Ta in reconstructing the experimental situation. By due consideration of the angle-dependent neutron spectrum of the ^{7}Li$(p,n)^{7}$Be reaction [19], the experimental time resolution, and the target-sample geometry, the TOF spectra can be reproduced reliably. In this way, the integral cross sections can be unfolded from the chosen TOF bins.

Calculated and measured TOF spectra for gold and tantalum are compared in Fig. 6, which illustrates the accuracy of these simulations. Small effects due to the energy spread of the proton beam and to the degradation of the neutron target were found to have negligible influence on this procedure.

Figure 7 shows the deduced ^{181}Ta cross section for the various TOF bins compared to the values corresponding to the precise measurement of Ref. [8]. The cross section can be reproduced down to channel 650 ($E_n=12$ keV). At lower energies, corresponding to the first arrival of backscattered neutrons at the target (Fig. 9), the scattering correction becomes dominant, thus hampering proper background subtraction. Therefore, the following analysis was restricted to TOF bins above channel 650.

The results for these bins are displayed in more detail in Fig. 8. The data points for the different converters and TOF bins are given relative to the calculated Ta cross sections. The corresponding cross section ratio

$$k=\frac{\sigma_m(\mathrm{Ta})}{\sigma_c(\mathrm{Ta})}$$

is plotted in Fig. 8, where σ_m denotes the measured and σ_c the calculated cross sections, respectively. The effective average cross sections were calculated using the well-known differential cross sections of ^{181}Ta [8] and ^{197}Au [19,28]. The error bars represent the counting statistics. The systematic uncertainties, mainly resulting from the efficiency correction Δ_ϵ, are illustrated by the deviations of the ratio k from unity and by the scatter of the data obtained with different converters.

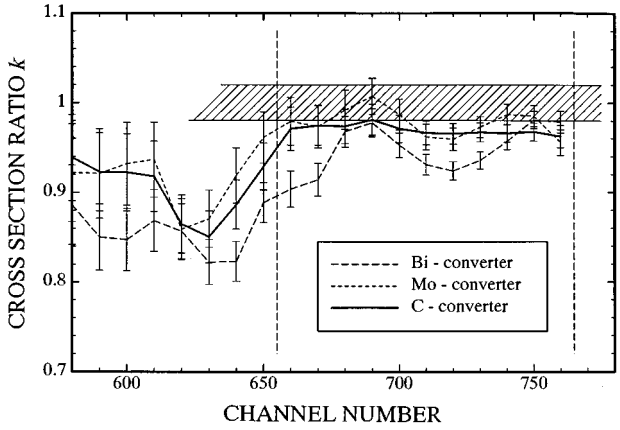

FIG. 8. The cross section ratio k for different converters. The shaded band represents the total uncertainty of the Ta cross section of Wisshak *et al.* [8], whereas the error bars of the present measurement indicate the statistical uncertainties only.

TABLE III. Samples for the Rb-measurement and related corrections.

		Samples			
		Au	^{87}Rb-I	^{87}Rb-II	Bi+C
Sample mass (g)		0.1017	1.58	1.09	2.05
Sample thickness (mm)		0.03	3	2	3
Sample diameter (mm)		15	15	15	15
Neutron binding energy S_n (MeV)		6.567	6.138	6.138	6.545
γ-ray self-absorption GA	Bi converter	0.994	0.986	0.991	0.949
	Mo converter	0.994	0.986	0.991	0.951
	C converter	0.995	0.988	0.992	0.957
Multiple scattering and self-shielding MS×SS		1.0	1.015	1.014	1.02
Δ_ϵ	Bi converter	–	0.961	0.961	0.988
	Mo converter	–	0.956	0.956	0.933
	C converter	–	1.022	1.022	0.944

F. Discussion

The cross sections found in the present experiment are slightly smaller than those obtained in the precise measurement of Wisshak *et al.* [8]. These deviations are consistent with the uncertainties of the efficiency correction Δ_ϵ. The data taken with the Bi converter exhibit the largest variations ($\pm 5\%$), whereas the data of the C converter follow an almost horizontal line in Fig. 8. Correspondingly, the results of the mixed Bi/C converter fall in between the two other data sets.

This behavior of the different converters follows from the measured efficiency curves (Fig. 3): The efficiency of the Bi converter deviates significantly from a linear increase of ϵ_γ in the energy range from 1 to 4 MeV, where the product of capture γ-ray intensity I_γ and detector efficiency ϵ_γ is largest. Therefore, variations of the capture γ-ray spectrum with neutron energy can produce a considerable effect. In contrast, the efficiency curve of the C converter is almost flat in this critical region, making it nearly insensitive to such variations. Accordingly, the C converter was found to be the best choice due to its almost ideal response function.

That the cross section ratio k of the C converter is practically constant for the different bins in Fig. 5 confirms the reliability of the procedures for treating the various corrections and the experimental backgrounds as well as the simulation of the TOF spectra. Averaged over the experimental spectrum and over the three converters, the precise measurement of Ref. [8] could be reproduced within 4%, thus confirming the 5–10% accuracy claimed for further experiments.

IV. MEASUREMENT OF THE ^{87}Rb CROSS SECTION

After the extensive tests of the improved Moxon-Rae setup, it was used to measure the small cross section of the neutron magic isotope ^{87}Rb. Because of their small (n,γ) cross sections, neutron magic nuclei are of particular interest for s-process nucleosynthesis since they act as bottlenecks in the reaction flow. Therefore, these data provide clues for the neutron exposure in the s process and determine the pronounced s-process maxima in the overall abundance distribution. Apart from this general aspect, ^{87}Rb is also important since it is situated in the very mass region where the weak and main s-process components, which are commonly assigned to helium burning in massive and in low mass stars, respectively, contribute about equally to the observed abundances. Moreover, ^{87}Rb is related to the interpretation of the s-process branching at ^{85}Kr [29,30].

A. Existing data and the aim of this measurement

The only differential (n,γ) cross sections for the rubidium isotopes have been reported by Beer and Macklin [31], who evaluated individual resonances in ^{85}Rb and ^{87}Rb up to neutron energies of 19 and 47 keV, respectively. At higher energies, average cross sections were given for certain energy bins with uncertainties of 4% for ^{85}Rb and 10% for ^{87}Rb. From these data, a stellar ^{87}Rb cross section of 21.5 mb was determined. Two other experiments [30,32] were performed via the activation technique, using the quasi-Maxwellian neutron spectrum of the ^{7}Li$(p,n)^7$Be reaction. Since the first of these measurements [32] yielded a very small stellar cross section of 11 ± 2 mb at $kT=30$ keV, the large discrepancy with respect to the differential data initiated a reinvestigation [30]. The improved cross section of this comprehensive study (18.0 ± 0.5 mb at $kT=30$ keV) was considered to be more reliable than the differential data

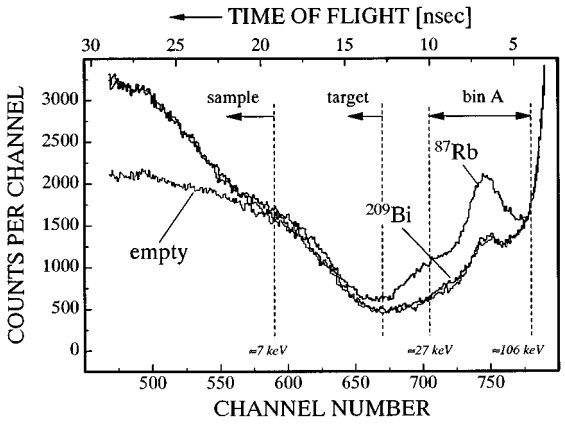

FIG. 9. Experimental TOF spectrum of the ^{87}Rb measurement taken with the Mo converter. This converter shows the strongest sensitivity to sample-scattered neutrons.

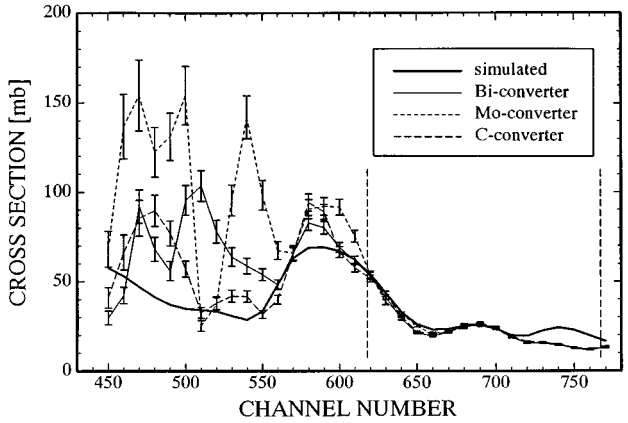

FIG. 10. Comparison of the integral cross section of the ^{87}Rb measurement from this work with the simulated cross section based on the data of Beer and Macklin [31].

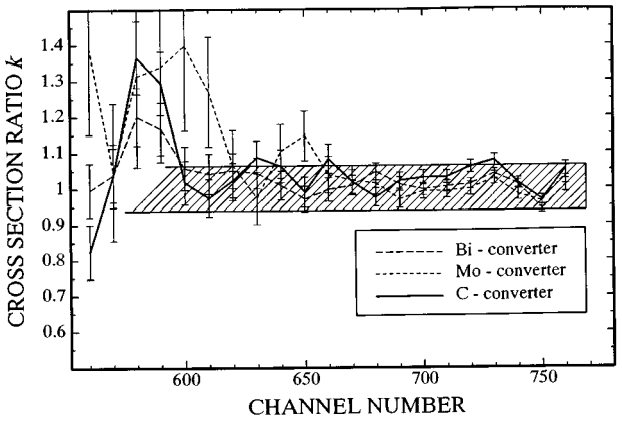

FIG. 12. The cross section ratio k for different converters. The shaded band represents the uncertainty of $\pm 7\%$, whereas the error bars of the present measurement indicate the statistical uncertainties only.

because the neutron scattering corrections were completely negligible in the activation measurement.

However, the activation technique can only provide an integral cross section for the experimental neutron spectrum. Since this spectrum represents an approximation of the true thermal spectrum, this method may lead to systematic effects if the cross section is dominated by resolved resonances (as for the neutron magic ^{87}Rb). Therefore, it was the aim of the present experiment to check the differential ^{87}Rb cross section, in particular in the energy region above 47 keV, where only average cross sections were given [31]. Since much smaller samples could be used and since neutron scattering corrections are significantly smaller, the improved Moxon-Rae setup provides an independent approach compared to the high resolution TOF method of Ref. [31].

B. Samples and experimental setup

The measurement was performed with a rubidium carbonate sample that was enriched in ^{87}Rb to 98.8%. The only isotopic impurity which contributed to the measured capture yield was the admixture of $1.2 \pm 0.5\%$ ^{85}Rb. Though hydroscopic, this compound was chosen because of its favorable nuclear properties. The original powder was pressed to pellets and covered with kapton foil in a dry argon atmosphere.

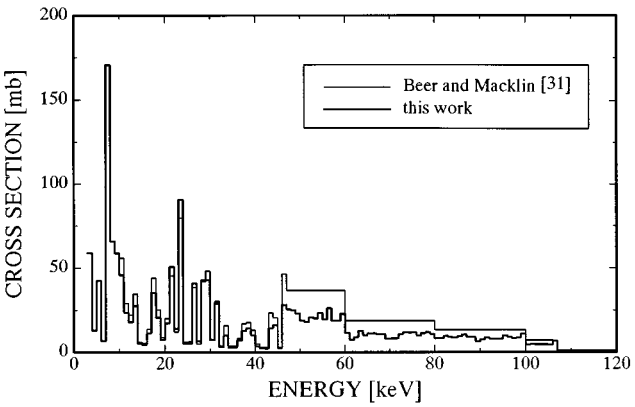

FIG. 11. Comparison of the differential ^{87}Rb cross sections of Beer and Macklin [31] with the data determined in this work.

To assure that the sample was free of water, the weight was controlled before and after the measurements. In addition, the rubidium content was determined at the end of the experiment by x-ray absorptiometry, yielding a sample mass within 0.3% of the value obtained via the sample weight.

The small level density of the neutron magic ^{87}Rb gave rise to difficulties in the calculation of the correction factor for neutron multiple scattering and self-shielding, MS$\times$SS, since the SESH code [20] is based on level statistics of the unresolved resonance region which may become a crude approximation for neutron magic nuclei in the keV region. Therefore, two ^{87}Rb samples of different thickness were used in the experiment for a direct test of these calculations.

The scattering sample was made of a mixture of Bi and C in order to simulate the scattering effect of $RbCO_3$. The relevant sample data are compiled in Table III.

The experimental setup and data acquisition were the same as in the Ta measurement, except that the flight path was increased to 23 ± 0.1 mm to account for the larger sample thickness. The total measuring time per sample was 40 h. Figure 9 shows the summed TOF spectra taken with the Mo converter, which exhibits the strongest sensitivity with respect to scattered neutrons. After background subtraction, the spectra were corrected for the ^{85}Rb impurity, which caused a sizable effect due to its much larger cross section. In this case, also the different capture γ-ray spectrum was considered [22,26].

Compared to the Ta case, the low neutron binding energy of ^{87}Rb results in smaller efficiency corrections Δ_ϵ (Table III) as well as in a reduced scatter of these values for the different converter materials.

C. Data analysis

The differential data of Ref. [31] were used for a first computation of the expected TOF spectra according to the prescription given for the Ta example. The calculated and measured cross sections are shown in Fig. 10. Even with the limited resolution of the present technique, several groups of strong resonances could be separated because of the low level density involved.

TABLE IV. Various contributions to the stellar neutron capture cross section of ^{87}Rb.

		Spectrum-averaged cross section for different kT (mb)				
Sample/converter	energy interval (keV)	12	20	30	40	50
Rb-I/Bi	10–106	23.3	20.2	18.0	16.7	16.0
Rb-I/Mo	10–106	24.0	20.5	18.2	17.0	16.4
Rb-I/C	10–106	24.0	20.8	18.6	17.4	16.7
Rb-II/Bi	10–106	22.1	19.6	17.6	16.4	15.7
Rb-II/Mo	10–106	21.7	19.0	17.0	15.8	15.1
Rb-II/C	10–106	23.3	20.1	17.9	16.7	15.9
Averaged	10–106	23.0±1.0	20.0±1.0	17.9±0.9	16.7±0.8	16.0±0.8
			Other contributions [a]			
^{85}Rb	10–106	324	266	231	213	203
^{87}Rb	0–10	59.2	59.3	59.8	60.1	60.3
^{87}Rb	10–106	21.7	21.2	20.6	20.1	19.7
^{87}Rb	106–∞	6.6	7.3	8.3	9.0	9.5

[a]Determined with data from Beer and Macklin [31].

While good agreement between measurement and simulation is obtained between channels 620 and 710, a significant discrepancy is found at higher energies, where the present spectrum does not contain any background from scattered neutrons. On the other hand this region corresponds to the energy interval where the differential data [31] were no longer analyzed in terms of resolved resonances. The first TOF bin that includes major contributions from the respective energy region above 47 keV ranges from channel 700 to 720 (Fig. 5).

In view of this discrepancy, the measured TOF spectrum was fitted by varying the differential cross sections of Ref. [31] in an iterative way. This calculation was performed for the energy region $10<E_n<106$ keV. Figure 11 shows the differential data [31] and the fitted cross section determined by minimizing the χ^2 values of all measured TOF spectra of both ^{87}Rb samples. This comparison shows clearly that our measurement agrees well with the differential data in the resolved resonance region, but that the previous data are consistently larger for neutron energies above 47 keV. This discrepancy may be due to an unrecognized scattering background in the previous data. We note that the present result, as plotted in Fig. 11, should be considered as an average over the energy bins of Ref. [31], the structure being completely due to the numerical iteration, which was carried out for 1 keV intervals. This structure is irrelevant for the final Maxwellian-averaged cross sections.

Figure 12 compares the cross section ratio k for the individual converters and using the improved cross section shape. The dashed area indicates a ±7% uncertainty of the calculated cross sections that was obtained by averaging over all Rb samples and detectors.

With the improved cross section shape, a new set of Maxwellian-averaged ^{87}Rb cross sections

$$\langle\sigma\rangle_{kT}=\frac{\langle\sigma v\rangle}{v_T}=\frac{2}{\sqrt{\pi}}\frac{\int\sigma(E)E\exp[-E/kT]dE}{\int E\exp[-E/kT]dE}$$

was calculated. In the energy regions $E_n<10$ keV and $E_n>106$ keV, which were not covered by the present experiment, the differential data of Beer and Macklin [31] were used.

The spectrum-averaged cross sections in the different energy regions are listed in Table IV. The upper part of this table shows the contribution from the interval between 10 and 106 keV which was derived from the individual TOF spectra. One finds that the results for the two ^{87}Rb samples agree within about 5%. This means that the uncertainty due to the correction for neutron multiple scattering and self-shielding might be of the same magnitude.

TABLE V. Stellar neutron capture cross section of ^{87}Rb.

Thermal energy (keV)	$\langle\sigma v\rangle/v_T$ (mb)			
	Walter *et al.* [32]	Beer and Macklin [31]	Raiteri *et al.* [30]	This work [a]
12				26.3±2.6
20		25.4		19.5±2.0
30	11±2	21.5	18.0±0.5	15.5±1.5
40		19.1		13.4±1.3
50		17.4		12.4±1.2

[a]A conservatively estimated uncertainty of ±10% is given for all cross section values.

The lower part of Table IV shows the average cross sections for the various energy intervals based on the differential data of Ref. [31], but normalized to the present results. These averages have still to be weighted with the Maxwell-Boltzmann spectrum in calculating the stellar cross sections which are summarized in Table V.

Because of the indirect method of data analysis, the systematic uncertainties cannot be determined by error propagation. In any case they will be dominated by the systematic uncertainties of the efficiency correction Δ_ϵ and by the multiple scattering and self-shielding corrections MS$\times$SS. Since these effects are represented by the differences obtained with the various converters and the two sample thickness, the final uncertainty was estimated by the spread of the respective results. An additional uncertainty of 0.5 mb was considered to account for the ^{85}Rb content of $1.2\pm0.5\%$.

The final stellar cross sections are given in Table V together with all previous data for $kT=30$ keV. The discrepancy with the differential data of Beer and Macklin [31] results from the smaller cross section of this work above 47 keV. The very low cross section of Walter *et al.* [32] was already recognized by Raiteri *et al.* [30] as being due to a wrong γ-ray intensity in the decay of ^{88}Rb. The difference to the cross section of 18 ± 0.5 mb at $kT=30$ keV reported in Ref. [30] itself was eventually understood after reanalyzing this measurement: It resulted from the fact that the difference between the quasi-Maxwellian spectrum used in the activation measurement and the true thermal spectrum was neglected in Ref. [30]. While this is an acceptable approximation for nuclei with a smooth energy dependence of the (n,γ) cross section, it is misleading in case of the neutron magic ^{87}Rb where the cross section shows a pronounced resonance structure even at high energies. With the proper correction, this effect reduces the result of Raiteri *et al.* [30] by 5–10%, thus providing excellent agreement with the present value.

V. CONCLUSIONS

A new setup of three Moxon-Rae detectors with different converters was constructed, and their γ-ray efficiency was experimentally determined up to an energy of 6.14 MeV. It was shown that the energy dependence of the γ-ray efficiency differs significantly from theoretical predictions due to previously neglected contributions from γ rays, which are directly interacting with the plastic scintillator and the photomultiplier.

With the experimental γ-ray efficiency, the described setup is well suited for the measurement of stellar neutron capture cross sections in cases where other techniques fail and where an accuracy of 5–10% is sufficient. The main advantage of the method is its excellent sensitivity which allows for TOF measurements of very small cross sections or with very small samples. This latter aspect is particularly important when only a small amount of sample material is available or for reducing the radiation hazard in investigations of radioactive samples.

It was found that the linear relationship between γ-ray efficiency and γ-ray energy of an ideal Moxon-Rae detector could not be realized with any of the converter materials C, Bi, Bi/C, and Mo. Of these, a carbon converter is most appropriate since it exhibits the best approximation of the requested proportionality between ϵ_γ and E_γ. Since the corresponding corrections can be much larger than assumed previously, a proper determination of the γ-ray efficiency up to the neutron binding energy of the investigated isotope is mandatory for achieving systematic uncertainties of less than 10%.

The improved Moxon-Rae setup was tested by measuring the well-known (n,γ) cross section of ^{181}Ta. It was found that the precise data of Wisshak *et al.* [8] could be reproduced within an inherent uncertainty of 5%. The first stellar cross section measured with this setup was that of ^{87}Rb, where a puzzling discrepancy between previous data could be resolved by the new value of $\langle\sigma v\rangle/v_T=15.5\pm1.5$ mb at a thermal energy of $kT=30$ keV.

Future applications are likely to concentrate on radioactive isotopes. In this respect, a Moxon-Rae setup exhibits a twofold advantage: In addition to the good overall efficiency which allows successful measurements even with mg samples, the detectors are practically insensitive to γ rays below 0.5 MeV, which helps to reduce the background due to the sample activity.

[1] J. Cowan, F.-K. Thielemann, and J. Truran, Phys. Rep. **208**, 267 (1991).
[2] B. Meyer, G. Mathews, W. Howard, and R. Hoffman, Astrophys. J. **399**, 656 (1992).
[3] F. Käppeler, H. Beer, and K. Wisshak, Rep. Prog. Phys. **52**, 945 (1989).
[4] R. Macklin, J. Gibbons, and T. Inada, Nucl. Phys. **43**, 353 (1963).
[5] K. Wisshak and F. Käppeler, Nucl. Sci. Eng. **77**, 58 (1981).
[6] K. Wisshak, F. Käppeler, G. Reffo, and F. Fabbri, Nucl. Sci. Eng. **86**, 168 (1984).
[7] M. Moxon and E. Rae, Nucl. Instrum. Methods **24**, 445 (1963).
[8] K. Wisshak, F. Voss, F. Käppeler, and G. Reffo, Phys. Rev. C **42**, 1731 (1990).
[9] K. Wisshak, K. Guber, F. Käppeler, J. Krisch, H. Müller, G. Rupp, and F. Voss, Nucl. Instrum. Methods A **292**, 595 (1990).
[10] K. Iyengar, B. Lal, and J. Jhingan, Nucl. Instrum. Methods **121**, 33 (1974).
[11] S. Malik, Nucl. Instrum. Methods **125**, 45 (1975).
[12] S. Malik and C. Majkrzak, Nucl. Instrum. Methods **130**, 443 (1975).
[13] F. Corvi, A. Prevignano, H. Liskien, and P. Smith, Nucl. Instrum. Methods A **265**, 475 (1988).
[14] M. Meyer, I. Venter, W. Coetzee, and D. Reitmann, Nucl. Phys. **A264**, 13 (1976).
[15] F. Corvi (private communication).
[16] M. Slawsky and H. Crane, Phys. Rev. **59**, 1203 (1939).
[17] K. Roulstin and S. Naqvi, Nucleonics **10**, 86 (1957).

[18] K. Wisshak and F. Käppeler, Nucl. Sci. Eng. **76**, 148 (1980).
[19] W. Ratynski and F. Käppeler, Phys. Rev. C **37**, 595 (1988).
[20] F. Fröhner, Technical report, Gulf General Atomic, 1968 (unpublished).
[21] E. Storm and H. Israel, Nucl. Data Tables **36**, 375 (1970).
[22] G. Reffo (private communication).
[23] G. Reffo, F. Fabbri, K. Wisshak, and F. Käppeler, Nucl. Sci. Eng. **80**, 630 (1982).
[24] M. Uhl and J. Kopecky, in *Nuclei in the Cosmos 1992*, edited by F. Käppeler and K. Wisshak (Institute of Physics Publishing, Bristol, 1993), p. 259.
[25] R. Macklin and J. Halperin, Phys. Rev. C **14**, 1389 (1976).
[26] S. Jaag, Master's thesis, University of Karlsruhe, 1990.
[27] S. Jaag and F. Käppeler, in *Nuclei in the Cosmos '90*, edited by H. Oberhummer and W. Hillebrandt (Max-Planck-Institut für Physik und Astrophysik, Garching, 1990), Vol. MPA/P4.
[28] R. Macklin (private communication).
[29] H. Beer, G. Walter, and F. Käppeler, Astrophys. J. **389**, 784 (1992).
[30] C. Raiteri, R. Gallino, M. Busso, D. Neuberger, and F. Käppeler, Astrophys. J. **419**, 207 (1993).
[31] H. Beer and R. Macklin, Astrophys. J. **339**, 962 (1989).
[32] G. Walter, H. Beer, F. Käppeler, and R.-D. Penzhorn, Astrophys. J. **339**, 962 (1986).